Mitochondrial-targeting Lonidamine-Doxorubicin nanoparticles for synergistic chemotherapy to conquer drug resistance

Mitochondrial Targeting Lonidamine-Doxorubicin Nanoparticles for Synergistic Chemotherapy to Conquer Drug Resistance

Yanqiu Liu,[+] *Xiujuan Zhang,*[+,*] *Mengjiao Zhou,*[+] *Xueyan Nan,*[+] *Xianfeng Chen,*[‡] *Xiaohong Zhang*[+,*]

[+]Institute of Functional Nano & Soft Materials (FUNSOM) and Jiangsu Key Laboratory for Carbon-Based Functional Materials & Devices, Soochow University, Suzhou Jiangsu, 215123 (P. R. China)

[‡]School of Engineering, Institute for Bioengineering, University of Edinburgh, Edinburgh EH9 3JL, United Kingdom.

Keywords： mitochondria targeting; triphenylphosphine; lonidamine; chemotherapy; drug resistance

Abstract

Lonidamine (LND) can act on mitochondria and inhibit energy metabolism in cancer cells and therefore has been used together with chemotherapy drugs for synergistically enhanced therapeutic efficacy. However, its use is hindered by the poor solubility and slow diffusion in the cytoplasm. To address these problems, we designed and prepared aqueous dispersible

nanoparticles (NPs) containing integrated components including triphenylphosphine (TPP) to target the mitochondria of cells and LND and doxorubicin (DOX) for synergistic cancer treatment and conquering drug resistance. This design allows the NPs to concentrate in the mitochondria of cells, solve the low solubility of LND, and contain very high load of LND and DOX in comparison with previously reported drug delivery systems based on various carrier nanomaterials. Detailed mechanism studies reveal that TPP-LND-DOX NPs could induce significant ROS production, mitochondrial membrane potential decrease and mitochondrial apoptosis pathway, thereby leading to great cytotoxicity in cancer cells. *In vivo* anticancer activities indicate that TPP-LND-DOX NPs exhibit the highest efficacy in tumor inhibition among all tested groups and show high effectiveness in drug resistant model. This work demonstrates the potential use of our TPP-LND-DOX NPs to jointly promote the mitochondria apoptosis pathway and contribute to conquer drug resistance in cancer therapy.

1. Introduction

Apoptosis is a process of programmed cell death[1-5] and primarily occurs via two pathways. One is the extrinsic cytoplasmic pathway elicited by the Fas death receptor, and the other is the intrinsic mitochondrial pathway in which the release of cytochrome-c from the mitochondria is first stimulated followed by activation of the death signal.[6,7] In recent years, mitochondrial apoptosis has been harnessed to arouse cancer cells suicide for cancer therapy.[8-10] For example, lonidamine (LND), a derivative of indazole-3-carboxylic acid, can effectively trigger the mitochondria apoptosis pathway by destroying the intrinsic transmembrane potential. One attractive characteristic of LND is that it can promote energy metabolism in normal cells but inhibit it in cancer cells.[11] Because of this, LND has been used in combination with other

anticancer drugs like doxorubicin (DOX) for improved therapeutic efficacy.[12-15] Despite of the promising feature, LND has low water solubility and slow diffusion in the cytoplasm. Therefore, very little LND can be delivered to tumor tissues and specifically to the mitochondria of cancer cells. To overcome these problems, mitochondria-targeting delivery systems have been broadly designed.[16-18] For instance, Zhang et al. synthesized copolymer containing mitochondria-targeting ligand triphenylphosphine (TPP) and LND, conjugated it to polyethyleneimine in chitosan-graft-PEI, and then prepared complexes of sizes of 85 to 180.4 nm with siRNA that target apoptosis inhibitor protein Bcl-2 in the mitochondria. These complexes were found to stimulate mitochondria apoptosis and could significantly increase cytotoxicity.[16] Li et al. developed liposomes of 80 nm in which LND and an anticancer drug epirubicin were encapsulated and delivered to mitochondria for potent co-therapy to treat drug-resistant cancer. In this system, dequalinium (DQA) was conjugated to the lipid bilayer membrane as a molecule for mitochondria targeting.[17] Although these drug delivery platforms are able to achieve mitochondria targeting and result in increased cancer therapy, one of the common problems is that the drug loading capacity and efficiency is rather low, because they all relying on additional carrier materials to deliver drugs. This will result in a large amount of materials accumulated in patient's body without therapeutic function and safety concern.

To improve drug loading capacity and therapeutic efficiency, we have performed extensive researches in which pure anticancer drugs are assembled to the form of nanoparticles, followed by coating with little amount of targeting ligands and stabilizing molecules.[19-23] The drug loading efficiency is typically over 90%. Inspired by these results, herein, we first synthesized copolymer TPP-LND and then co-assemble it with a very commonly used anticancer drug doxorubicin (DOX) to form multidrug nanoparticles (NPs) (donated TPP-LND-DOX NPs). To enable their

stability, these NPs were modified with mPEG-COOH. The PEGylated TPP-LND-DOX NPs are electrically neutral and possess high water dispersity and bio-environmental stability. In the design, TPP is to lend the NPs with mitochondria targeting ability. DOX is not only for chemotherapy but also used for bioimaging due to its strong fluorescence, and LND is to trigger mitochondria apoptosis and enhance the therapeutic efficacy of DOX. We systematically investigated the morphology, size, composition, and stability of TPP-LND-DOX NPs and tested them *in vitro* mitochondria targeting, cytotoxicity, and the mechanism of apoptosis, and *in vivo* blood circulation, biodistribution and therapeutic function. Our results demonstrate that these NPs without additional drug carrier material can specifically target mitochondria and effectively conquer the drug resistance of DOX-resistant MCF-7/ADR cells, thereby obtaining greatly enhanced tumor inhibition effect. These results highlight the great potential of these mitochondria targeting multidrug NPs for highly efficient synergistic chemotherapy towards inhibition against drug resistances.

2. Results and discussion

2.1. Synthesis, preparation and characterization of TPP-LND-DOX NPs

The synthetic route of TPP-LND is shown in **Scheme 1**. The (2-aminoethyl)triphenylphosphonium bromide (TPP-NH_2) was first synthesized according to a previously published method,[24] and then TPP-LND was obtained through the reaction between the TPP-NH_2 and LND. The product was verified using ^{1}H NMR (Figure S1). The conjugation of TPP is to lend the ability of our drug delivery platform to target the mitochondria of cancer cells.

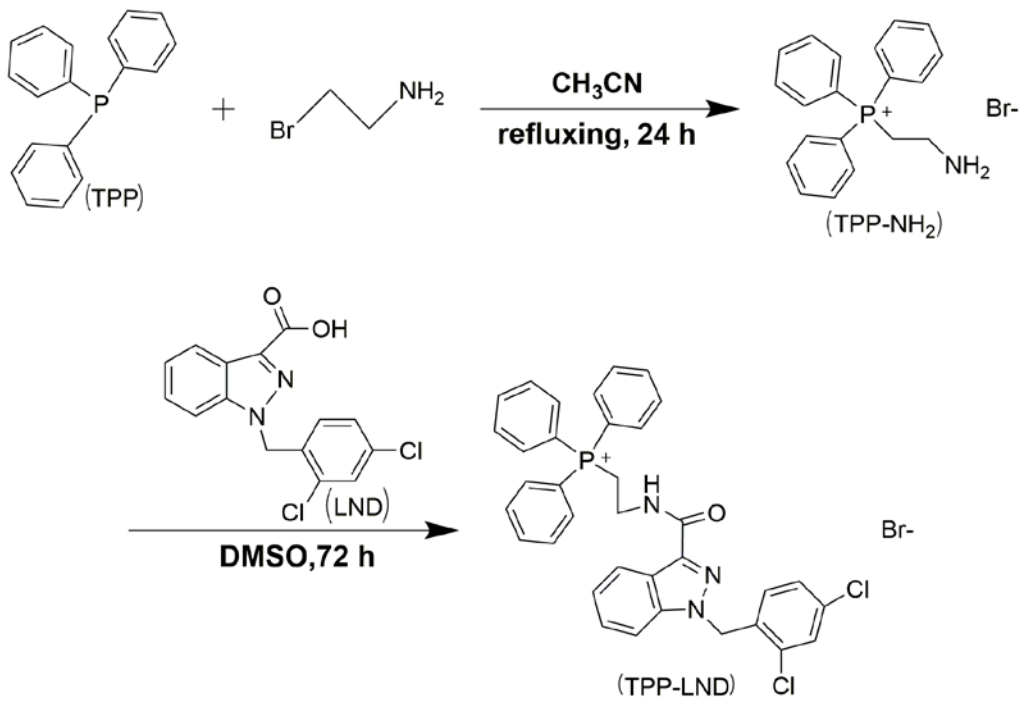

Scheme 1. The synthetic route of TPP-LND.

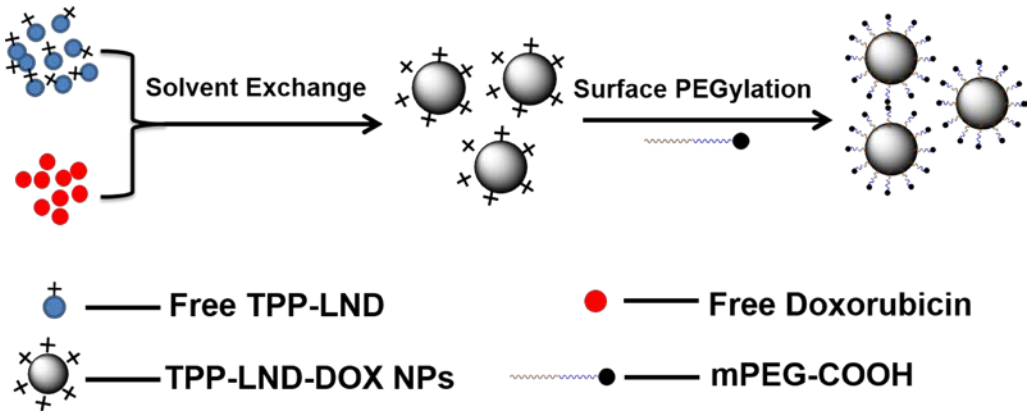

Scheme 2. The synthetic procedure and surface modification of TPP-LND-DOX NPs.

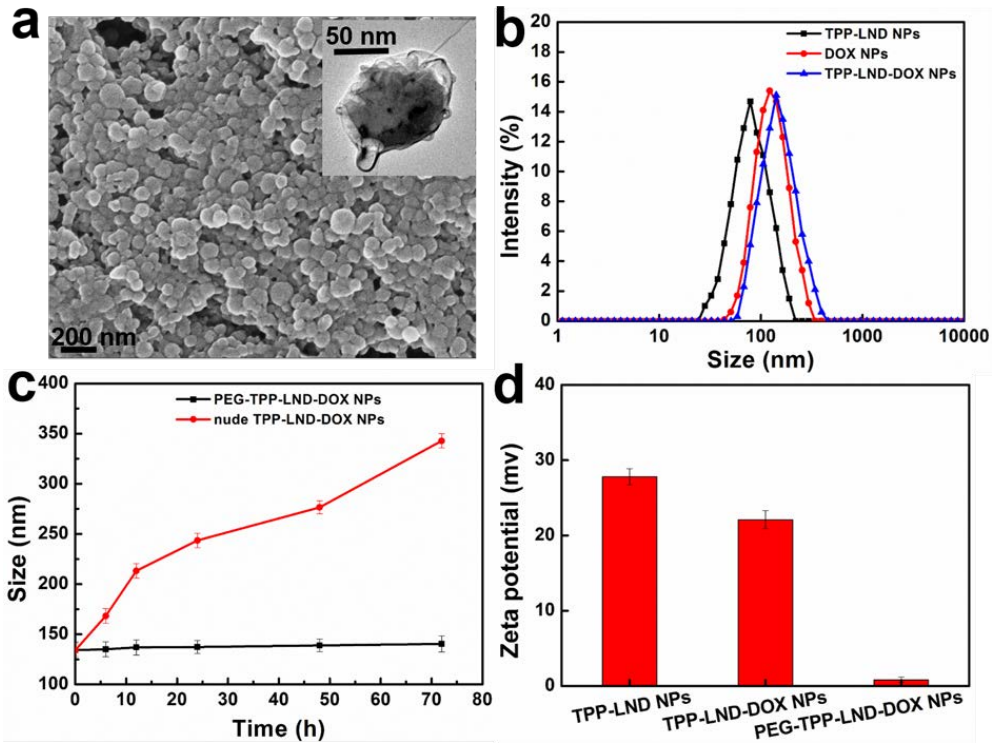

Figure 1. (a) The SEM image of TPP-LND-DOX NPs. Inset: TEM image of an individual TPP-LND-DOX NPs. (b) The DLS size analysis of TPP-LND NPs, DOX NPs, and TPP-LND-DOX NPs. (c) The size evolution of TPP-LND-DOX NPs in PBS before and after surface modification by mPEG-COOH. (d) The Zeta potentials of TPP-LND NPs, TPP-LND-DOX NPs, and PEG-TPP-LND-DOX NPs.

After synthesis of TPP-LND, TPP-LND-DOX NPs were prepared via a solvent exchange method (**Scheme 2**). In the preparation, hydrophobic DOX molecules were produced by adding triethylamine (TEA) to hydrophilic DOX•HCl in dimethyl sulfoxide (DMSO).[19] Subsequently, TPP-LND-DOX NPs were produced by simultaneous injection of 200 μL of TPP-LND/MeOH solution and 150 μL of DOX/DMSO solution into 5 mL of aqueous water under stirring. This process will result in multi-drug NPs with a positive surface charge. The scanning electron microscopy (SEM) and transmission electron microscopy (TEM) images in

Figure 1a show that the as-prepared TPP-LND-DOX NPs are spherical in shape and have approximately uniform size. The elemental compositions of nude TPP-LND-DOX NPs were determined by energy-dispersive X-ray spectroscopy (EDX) (Figure S2). The ^{1}H NMR spectrum in Figure S3 further confirms the successful preparation of TPP-LND-DOX NPs. The dynamic light scattering (DLS) analysis (**Figure 1b**) shows the mean size of TPP-LND-DOX NPs is about 110 nm, larger than TPP-LND NPs (about 80 nm) and DOX NPs (about 100 nm) that were also prepared from solvent-exchange method. To improve their stability of TPP-LND-DOX NPs, mPEG-COOH was then applied to modify the surface of NPs and convert the surface charge to be neutral (PEG-TPP-LND-DOX NPs). The stability of TPP-LND-DOX NPs in phosphate buffered saline (PBS) before and after surface modification is presented in **Figure 1c**. It is clear that the PEG modified NPs are very stable with no measurable size change over 72 hours observation, while the size of bare TPP-LND-DOX NPs without surface modification sharply increases in the same period. We further studied the release profiles of DOX from TPP-LND-DOX NPs and PEG-TPP-LND-DOX NPs at different pHs (Figure S4). The results reveal that DOX rapidly releases from TPP-LND-DOX NPs, but the release rate is significantly slower at neutral pH after surface modification with PEG. As presented in **Figure 1d**, the zeta potentials of TPP-LND NPs, TPP-LND-DOX NPs, PEG-TPP-LND-DOX NPs are about +27.8, +21.9 and +0.7 mv, respectively.

2.2 *In vitro* cellular uptake and bioimaging

We designed TPP-LND-DOX NPs with the desire to target mitochondria and consequently achieve potent therapeutic efficacy. Therefore, it is essential to first investigate whether these NPs can indeed reach mitochondria. To know this, the intracellular uptake of TPP-LND-DOX NPs in HeLa cells was observed using confocal fluorescence microscopy. For comparison, the

cellular uptake of the mixture of free TPP-LND and DOX molecules (TPP-LND+DOX) was also studied. DOX plays a role as fluorescent probe due to its inherent fluorescence. As presented in **Figure 2**, the fluorescence signal of DOX molecules in the control group is stronger than that of the TPP-LND-DOX NPs group at 4 h after incubation with HeLa cells. The reason is that free DOX and NPs have different cellular uptake mechanisms. It is well known that DOX molecules are able to diffuse through the cell membranes, while NPs are uptaken through endocytosis.[22] After being internalized, the DOX molecules in the control group begin to enter the nuclei of the HeLa cells at 4 h post incubation and the amount in the nuclei continuously increases with time. In great contrast, almost all of the DOX molecules in the TPP-LND-DOX NPs group accumulate in the mitochondria, barely entering the nucleus till after 16 h incubation. By 24 h (Figure S5), it can be seen that nearly all of the DOX molecules in the control group are in the nuclei, while the DOX in the TPP-LND-DOX NPs group still remain in the mitochondria. These results clearly demonstrate that our TPP-LND-DOX NPs are able to target the mitochondria of cells and this lays the foundation of improved cytotoxicity in cells and effective therapeutic efficacy in animal tumor model. We also compared the *in vitro* cellular uptake of TPP-LND-DOX NPs with or without surface modification (Figure S6). From the images in both groups, it can be found that TPP-LND-DOX NPs are able to target mitochondria, demonstrated by the colorization (yellow) of NPs (red) and mitochondria (green). These experimental data clearly confirm that the modification of PEG on NPs will not influence the targeting ability of TPP.

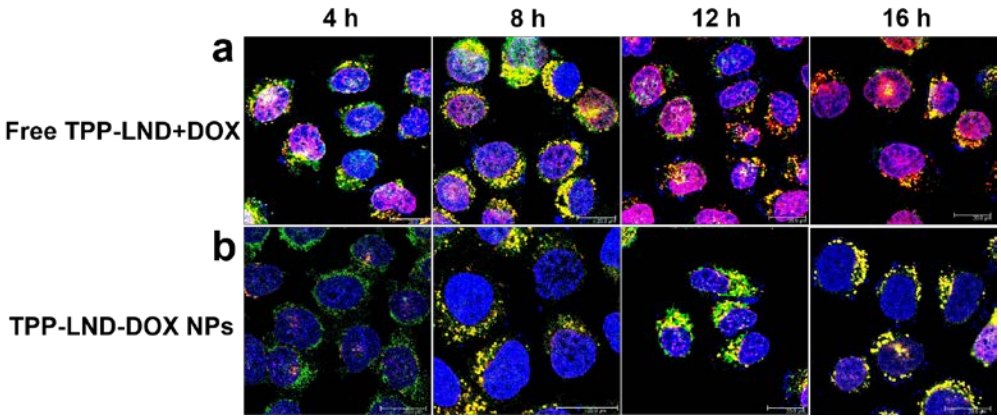

Figure 2. Cellular uptake and intracellular distribution of the mixture of free TPP-LND and DOX molecules (TPP-LND+DOX) and TPP-LND-DOX NPs in HeLa cells. The confocal fluorescence microscopy images of intracellular localization of the NPs in HeLa cells were observed at 4, 8, 12, and 16 h incubation with free TPP-LND+DOX and TPP-LND-DOX NPs at the same concentration. Scale bar: 20 μm. Hoechst 33258 and Mito-Tracker Green were used to stain the nuclei and mitochondria of cells, respectively. NPs, mitochondria and nucleus are shown in red, green, and blue, respectively.

2.3 *In vitro* cytotoxicity

Once confirm TPP-LND-DOX NPs can successfully target the mitochondria of cells, we then investigated their effect on cancer cells. Four groups of mouse breast cancer cell lines (4T1) were individually incubated with DOX NPs, TPP-LND NPs, mixture of free TPP-LND and DOX molecules (TPP-LND+DOX), and TPP-LND-DOX NPs. After 48 h incubation, it is evident that, at all concentrations, TPP-LND-DOX NPs always exhibit significantly higher cytotoxicity than other 3 groups (Figure S7). Following this success, we next studied the efficacy of TPP-LND-DOX NPs in overcoming drug resistance. First, human breast cancer cells (MCF-7) and DOX-resistant MCF-7/ADR cells were cultured with free DOX molecules for 24 and 48 h (Figure S8).

It is obvious that the cytotoxicity of DOX molecules on MCF-7/ADR cells is lower than that on MCF-7 cells. Second, the two cancer cell lines were cultured with the same 4 groups of materials as used for 4T1 cells for 24 and 48 h (**Figure 3 and S9**). For MCF-7 cells, DOX NPs exhibit moderately higher cytotoxicity than TPP-LND NPs at all concentrations (**Figure 3a** and **3b**). However, as shown in **Figure 3c** and **3d**, there is an opposite phenomenon for MCF-7/ADR cells for these two materials. In other words, at all concentrations, the cytotoxicity of TPP-LND NPs is better than DOX NPs. With 48 h incubation, the proliferation rate of MCF-7 and MCF-7/ADR cells treated with TPP-LND-DOX NPs is always the lowest in all studied groups. Notably, TPP-LND-DOX NPs can very efficiently kill drug resistant cancer cells. After 48 h incubation, the viability of MCF-7/ADR cells treated by TPP-LND-DOX NPs at the concentration of 12 μg/mL is as low as 22.3%. In comparison, the viabilities of MCF-7/ADR cells treated by DOX NPs and TPP-LND NPs are 60.2% and 47.6%, respectively. This is in line with the previous finding that the combination of LND and epirubicin can dramatically improve the efficacy of overcoming drug resistant cancer.[17] We also compared the cytotoxicity of free LND and covalently conjugated TPP-LND by MTT assay (Figure S10). It can be seen from the figure that TPP-LND exhibits higher cytotoxicity than LND in both MCF-7 cells and MCF-7/ADR cells (the concentrations of LND were maintained the same in both groups, ranging from 0 to 32 μg/mL). In addition, we investigated the cytotoxicity to normal cells. Surprisingly, the cytotoxicity of DOX NPs, TPP-LND NPs, TPP-LND+DOX, and TPP-LND-DOX NPs on normal human liver cells (HL7702) is significantly lower than that on cancer cells (Figure S11).

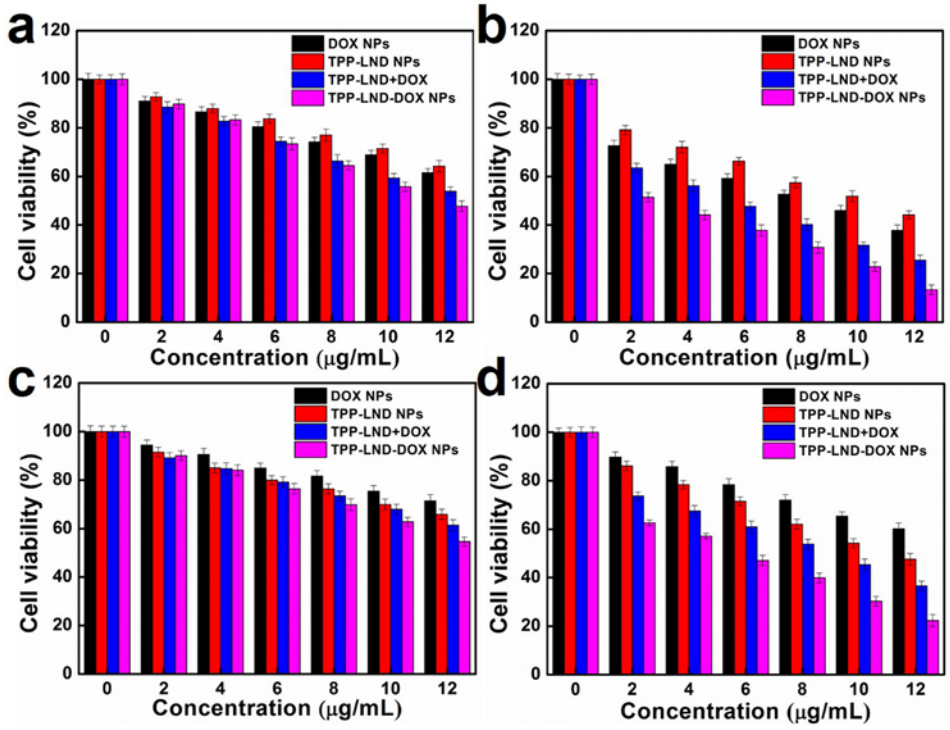

Figure 3. (a) and (b): Cell viabilities of MCF-7 cells after 24 (a) and 48 (b) h incubation with DOX NPs, TPP-LND NPs, mixture of free TPP-LND and DOX molecules (TPP-LND+DOX), and TPP-LND-DOX NPs. (c) and (d): Viabilities of MCF-7/ADR cells after 24 (c) and 48 (d) with DOX NPs, TPP-LND NPs, TPP-LND+DOX, and TPP-LND-DOX NPs. The concentrations of both LND and DOX were maintained to be the same, with a range from 0 to 12 μg/mL.

2.4 Detection of intracellular generate reactive oxygen species (ROS)

After knowing that TPP-LND-DOX NPs can efficiently kill cancer cells, we carried out studies to explore the mechanisms. Mitochondria are the primary site to generate ROS within cells, so we firstly investigated if the targeted delivery of drugs to mitochondria led to production of significant level of ROS.[25-29] In order to measure the content of ROS in cells after stimulation with TPP-LND-DOX NPs, DCFH-DA was chosen as the ROS probe. 4T1 cells were incubated

with DOX NPs, TPP-LND NPs, mixture of free TPP-LND and DOX molecules (TPP-LND+DOX), and TPP-LND-DOX NPs for 12 and 24 h. The cells cultured in blank medium were investigated for comparison. The results are presented in Figure 4, in which stronger fluorescence intensity indicates higher level of ROS generation. Evidently, TPP-LND-DOX NPs induce much higher amount of ROS than other materials. We also tested the ROS generation in MCF-7/ADR cells cultured with the same material for the same duration (Figure S12), the results are in conformance with the above.

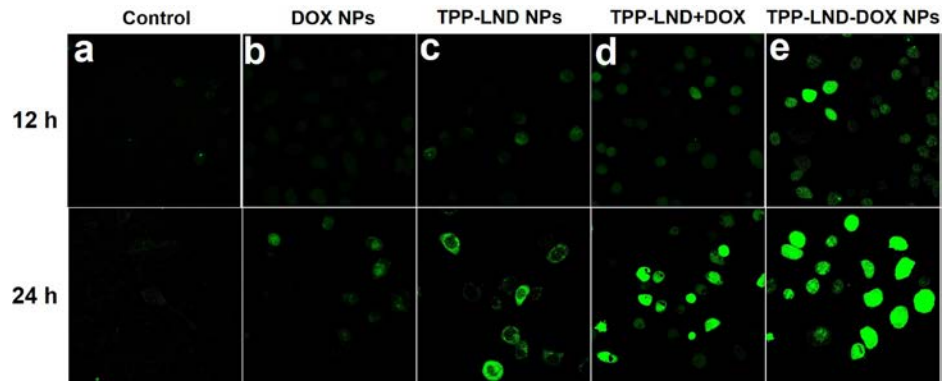

Figure 4. Reactive oxygen species (ROS) generation in 4T1 cells treated with different drugs. ROS generation was detected with DCFH-DA. DCFH-DA can turn to highly fluorescent product upon oxidation. Therefore, the ROS generation was investigated with confocal fluorescence microscopy and stronger fluorescence intensity indicates more ROS production. The confocal fluorescence microscopy images of (a) untreated cells, and the cells incubated with (b) DOX NPs, (c) TPP-LND NPs, (d) free TPP-LND and DOX molecules (TPP-LND+DOX), and (e) TPP-LND-DOX NPs for 12 and 24 h. Scale bar: 20 μm. The concentrations of both LND and DOX were maintained at 10 μg/mL.

2.5 Mitochondrial membrane potential (Δψm) depolarization

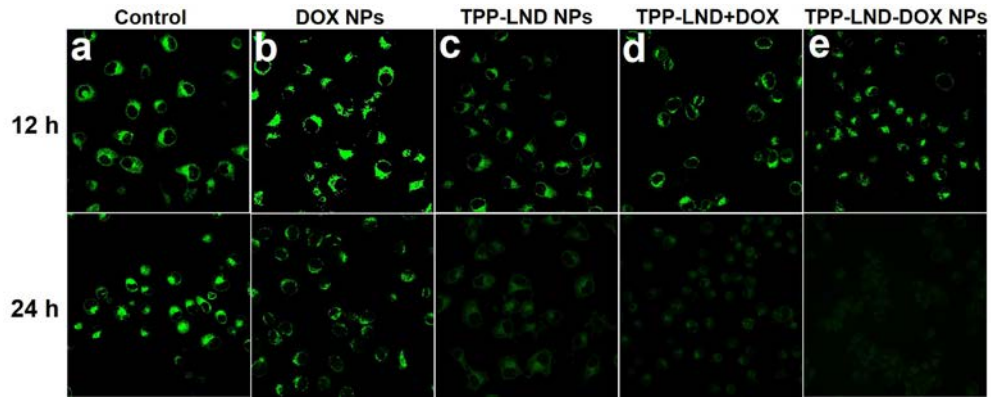

Figure 5. The mitochondrial membrane potential (Δψm) depolarization of 4T1 cells was detected with Rhodamine 123. 4T1 cells were observed at 12 and 24 h incubation with (b) DOX NPs, (c) TPP-LND NPs, (d) free TPP-LND and DOX molecules (TPP-LND+DOX), and (e) TPP-LND-DOX NPs. (a) The control experiment. Scale bar: 20 μm. The concentrations of both LND and DOX were maintained at 10 μg/mL.

The generation of ROS has very close relation with the mitochondrial membrane potential and LND has been demonstrated to have effect on the mitochondria potential.[30] Therefore, our next step was to explore the membrane potential when cells were treated with TPP-LND-DOX NPs. 4T1 cells were cultured with DOX NPs (group (b)), TPP-LND NPs (group (c)), free TPP-LND and DOX molecules (TPP-LND+DOX, group (d)), and TPP-LND-DOX NPs (group (e)) for 12 and 24 h. The cells in blank medium were studied as a control. Then the cells were stained with Rhodamine 123 for 30 min. Rhodamine 123 is a lipophilic cation dye and can be accumulated by mitochondria in a membrane potential change dependent manner. Once accumulated, the fluorescence is quenched. As presented in **Figure 5**, after 12 h incubation, the fluorescence intensity of group (e) decreases compared with control group, indicating that the Δψm has decreased. At 24 h, all of the Δψm of four drug groups treated cells have different degrees of

weakening of fluoresce intensity, while the Δψm of the group (e) decreased sharply. This phenomenon also occurs in MCF-7/ADR cells (Figure S13). Previous studies have also shown that the application of DOX and LND can lead to decreased mitochondrial membrane potential.[31-33]

2.6 Synergistic effect on cell apoptosis

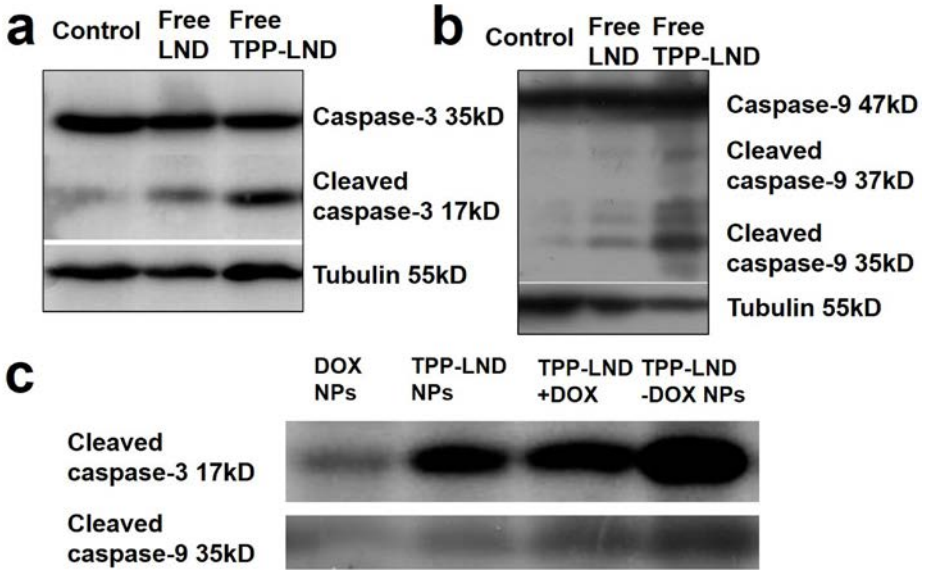

Figure 6. The expression of caspase-3 (a) and caspase-9 (b) of 4T1 cancer cells upon incubation with different materials including free LND, and free TPP-LND. (c) The expression of caspase-3 and caspase-9 of 4T1 cancer cells after treatment with DOX NPs, TPP-LND NPs, the mixture of free TPP-LND and DOX molecules (TPP-LND+DOX), and TPP-LND-DOX NPs for 24 h. The concentrations of both LND and DOX were maintained at 10 μg/mL.

As we know, the mitochondrial intrinsic pathway is one of the two principal pathways leading to cell apoptosis. In this pathway, an apoptotic trigger firstly target mitochondria and trigger the

release of cytochrome-c from the mitochondria, which is consequently able to activate Apaf-1 (apoptotic protease-activating factor-1) that recruits caspase-9 and ultimately activates caspase-3,[1,34,35] resulting in a final pathway to cell apoptosis. To explore if this is the mechanism of cell death in our work, different groups of 4T1 cells were incubated with different materials including free LND, free TPP-LND, DOX NPs, TPP-LND NPs, mixture of free TPP-LND and DOX molecules (TPP-LND+DOX), and TPP-LND-DOX NPs for 24 h. Then, the expressions of caspase-3 and caspase-9 were measured through Western blot (**Figure 6**).

Cleaved caspase-3[36] is the active form of caspase-3 and acts as an early marker of apoptosis. For caspase-9,[37] although the cleavage is not necessary for activation, the intrinsic cell death is always associated with it. As presented in **Figure 6a** and **6b**, the expression of cleaved caspase-3 and caspase-9 under the action of free TPP-LND is unambiguously more than that of the free LND group. This is very likely because TPP-LND reaches mitochondrial and activates the pathway to express caspase-9 and caspase-3. In **Figure 6c**, the amount of activated caspase-3 and caspase-9 rises remarkably in the 4T1 cells treated with TPP-LND-DOX NPs in comparison with that of other groups, which suggests that the mitochondria apoptosis pathway has been triggered. Overall, as sketched in **Scheme 3**, our findings firmly corroborate the conclusion that TPP, LND, and DOX in the TPP-LND-DOX group synergistically promote an apoptosis cascade via the intrinsic mitochondrial pathway.

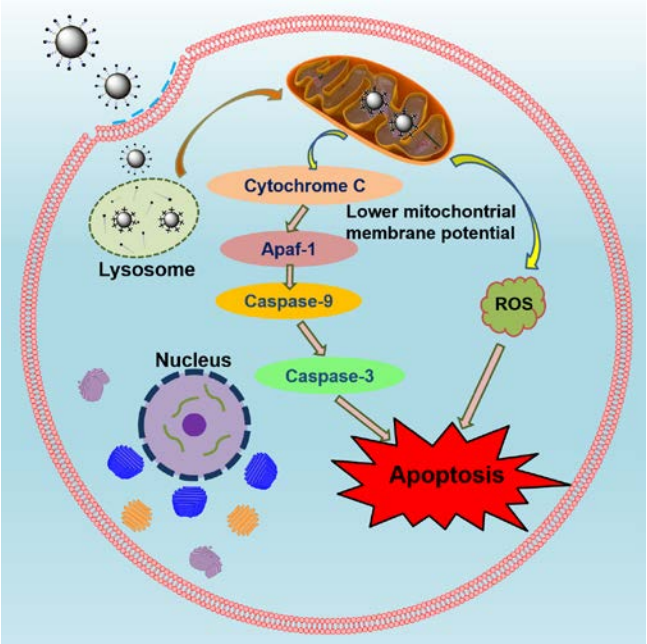

Scheme 3. Sketch of the mechanism of the intrinsic mitochondria apoptosis pathway co-triggered by the mitochondria targeting delivery of TPP-LND-DOX NPs.

2.7 Blood circulation and biodistribution

In order to find out the applicability of PEG-TPP-LND-DOX NPs for *in vivo* tumor targeted therapy, we administered PEG-TPP-LND-DOX NPs into nude BALB/c mice through intravenous injection and explored their concentrations in blood over time through measuring the fluorescence of DOX. The blood's autofluorescence was subtracted from the fluorescence intensities of the blood samples containing the injected NPs. As displayed in **Figure 7a**, making DOX in the form of NPs is able to prolong its half-life to approximately 2 h in blood circulation. This is significantly longer than the circulation half-life of free DOX molecules of less than 10 min.[22] The well extended blood circulation time could boost the delivery of drugs to tumor sites via the EPR effect.

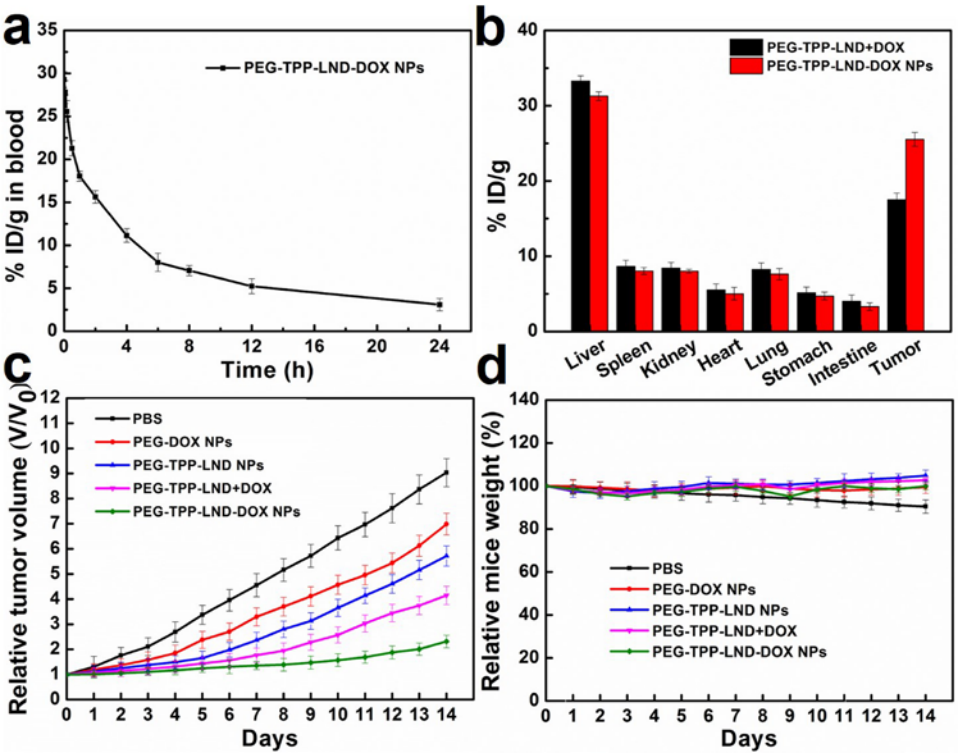

Figure 7. (a) The evolution of the concentration of PEG-TPP-LND-DOX NPs over time. (b) The biodistribution of the mixture of free PEG-TPP-LND and DOX (PEG-TPP-LND+DOX), and PEG-TPP-LND-DOX NPs in major organs and tumor tissues at 24 h after injection. (c) The tumor volume of MCF-7/ADR tumor bearing nude BALB/c mice at different times after treatment with saline, PEG-DOX NPs, PEG-TPP-LND NPs, PEG-TPP-LND+DOX, and PEG-TPP-LND-DOX NPs. The both concentrations of LND and DOX were maintained at 1 mg/mL. (d) The mouse body weight change with time.

The biodistribution of administered NPs was also explored. We injected 2 groups of materials including the mixture of free PEG-TPP-LND and DOX molecules (PEG-TPP-LND+DOX) and PEG-TPP-LND-DOX NPs intravenously into MCF-7/ADR tumor bearing nude BALB/c mice, and the fluorescence levels of DOX in different organs and tumors were detected after 24 h. The fluorescence intensity of each organ was calibrated by subtracting its autofluorescence. In

Figure 7b, at 24 h post NPs injection, the fluorescence intensity in tumor sites of the mice treated with PEG-TPP-LND-DOX NPs (25.8% ID/g) is much higher than that of the mice injected with PEG-TPP-LND+DOX (17.4% ID/g). This outcome is very likely due to: (1) the long blood circulation of PEG-TPP-LND-DOX NPs and the "enhanced permeability and retention" (EPR) effect result in passively targeted delivery to tumor sites; (2) the surface modification of PEG helps the drugs to better escape the "reduced reticuloendothelial system" (RES) organs.[38]

2.8 *In vivo* anticancer activities

Once we know that TPP-LND-DOX NPs can target mitochondria and induce high toxicity, have long blood circulation life, and are able to increase the delivery to tumor sites, the key question will be whether these advantages can transfer to potent *in vivo* anticancer therapy. Therefore, we investigated the *in vivo* therapeutic efficacy of TPP-LND-DOX NPs using the MCF-7/ADR tumor model on nude BALB/c mice. There were 5 groups of mice in our study including: (1) PBS control group; (2) PEG-DOX NPs group; (3) PEG-TPP-LND NPs group; (4) the mixture of free PEG-TPP-LND and DOX molecules group (PEG-TPP-LND+DOX); (5) PEG-TPP-LND-DOX NPs group. In each group, 200 μL of drug dose of 1 mg/mL were intravenously administered at day 0 and 7. The tumor sizes and body weights of mice were measured daily for two weeks. **Figure 7c** shows that the tumor sizes in PBS control group rapidly increase by 9.11 ± 0.56 fold during the 2-week experimental period. Both DOX NPs and TPP-LND NPs are able to inhibit tumor progress to some extent, indicated by the volume increase of 6.92 ± 0.36 and 5.34 ± 0.41 fold, respectively. The therapeutic efficacy of TPP-LND NPs is moderately better than that of DOX NPs, mainly due to the DOX-resistant cancer cells in this tumor model. The combination of TPP-LND and DOX can further improve tumor inhibition,

demonstrated by the tumor volume increase of 4.02 ± 0.32 fold. In comparison, it is very appealing that TPP-LND-DOX NPs have the highest efficacy in tumor inhibition and the tumor volume increase is only 2.17 ± 0.23 fold. This clearly proves that the superior characteristics of TPP-LND-DOX NPs can lead to potent anticancer therapy.

To use nanomedicine, beyond high therapeutic efficacy, it is also necessary to consider its biocompatibility. Undesired side effects to normal tissues have always been one of the great concerns in development of nanomedicines.[39,40] As a preliminary indicator, we measured the body weight of mice daily to evaluate the toxicity of the treatments throughout the therapeutic period. As **Figure 7d** displayed, the mice body weight treated with PBS keeps falling, while the mice of other treated groups show a gentle decrease of body weight (< 10%) after drug administration, but then get steady weight increase, indicating low side effects.

3. Conclusion

In summary, we designed and synthesized multifunctional TPP-LND-DOX NPs and applied them to *in vitro* and *in vivo* cancer treatment. The cellular uptake study indicates that TPP-LND-DOX NPs could accumulate selectively in the mitochondria of cancer cells with the active targeting of TPP. The *in vitro* experiment results prove that TPP-LND-DOX NPs are able to induce generation of significant amount of ROS and obvious $\Delta\psi m$ decrease, thereby leading to significant death of cancer cells. Besides the therapeutic effect, DOX in TPP-LND-DOX NPs could also be used as a fluorescent probe due to its strong fluorescence. With this, NPs' specific accumulation in mitochondria of cancer cells can be clearly distinguished. PEGylated TPP-LND-DOX NPs possess good biocompatibility, high stability, extended blood circulation time and intense accumulation in tumors. Owing to these superior characteristics, TPP-LND-DOX NPs exhibit significantly improved anticancer therapeutic efficacy and reveal much higher

cytotoxicity than other treatment groups both in *in vitro* and *in vivo* studies, indicating the synergistic effect. More importantly, *in vivo* anticancer activities study demonstrates that TPP-LND-DOX NPs are very effective in overcoming the DOX-resistance of cancer cells and showing effective tumor inhibition in drug resistant tumor model, with no obvious side effect. Overall, these multifunctional TPP-LND-DOX NPs could realize real time imaging, efficient mitochondria targeting, increased delivery to tumor, and high efficiency in killing DOX-resistant cancer cells and inhibiting tumor growth.

4. Experiments

4. 1. Materials

Lonidamine, doxorubicin (DOX•HCl) were purchased from Beijing InnoChem Science & Technology Co., Ltd. Triphenylphosphine (TPP), 2-bromoethylamine hydrobromide, dimethyl sulfoxide-d_6 (DMSO-d_6), 1-(3-dimethylaminopropyl)-3-ethylcarbodiimide hydrochloride (EDC), ethanol, methanol (MeOH), triethylamine (TEA), dichloromethane (DCM), sodium hydroxide (NaOH), sodium chloride (NaCl), dimethylsulfoxide (DMSO), petroleum ether were ordered from Sinopharm Chemical Reagent Beijing Co., Ltd. 4-dimethylaminopyridine (DMAP), anhydrous acetonitrile (CH_3CN), anhydrous dimethyl sulfoxide were ordered from J&K Scientific Ltd.

4. 2. Synthesis of $[Ph_3PC_2H_4NH_2]^+Br^-$ (TPP-NH_2)

(2-aminoethyl)triphenylphosphonium bromide (TPP-NH_2) was obtained by the reaction between $BrCH_2CH_2NH_3^+Br^-$ (2.049 g, 10 mmol) and TPP (2.621 g, 10 mmol) in CH_3CN (40 mL), steered and refluxed for 24 h. Then, the reaction mixture was rotor-evaporated, and the rest

of the crystals were dissolved in minimal amount of H_2O, the aqueous solution was adjusted with NaOH (2 mol/L) to pH 11.0. Thereafter, the water was rotor-evaporated and the amine was extracted with MeOH. After filtering NaBr, 2.41 g (Yield, 40%) TPP-NH_2 precipitated from the methanolic filtrate triturated with diethyl ether. This method was performed as described previously.[24]

4. 3. Synthesis of TPP-LND

Lonidamine (LND, 1.927 g, 6 mmol), 4-dimethylaminopyridine (DMAP, 0.733 g, 6 mmol) and 1-(3-dimethylaminopropyl)-3-ethylcarbodiimide hydrochloride (EDC, 1.150 g, 6 mmol) were dissolved in anhydrous DMSO (20 mL) and steered for 6 hours. TPP-NH_2/CH_3CN solution was added next, steering for 72 hours. After that, the solution was extracted with mixed solution of methylene chloride and ultrapure water (methylene chloride: ultrapure water = 5: 1), and then washed with saturated salt water, added a certain amount of anhydrous sodium sulfate (Na_2SO_4), standing overnight. Next, filtered and evaporated the filtrate, the remaining crystals were dissolved in a lot of water, freeze-dried at -80 °C to afford 1.277 g TPP-LND (Yield, 35%).

4. 4. Preparation and surface modification of DOX NPs, TPP-LND NPs, and TPP-LND-DOX NPs

All NPs were synthesized according to our previously reported method.[41] In the method, we first prepared DOX NPs. In the preparation, 40 μL TEA was added into 10 mL of 3 mg/mL hydrophilic DOX•HCl/DMSO solution under moderate stirring at room temperature, getting hydrophobic DOX molecules after 3 h. For preparing DOX NPs, 200 μL of DOX/DMSO solution were added into 5 mL of petroleum ether and kept stirring at 900 rpm for 6 min. Then 2 ml of water was added to 1 ml of the prepared DOX NPs solution in petroleum ether followed by

filtering with a 10 KD ultrafiltration cube for 10 min twice to obtain DOX NPs in aqueous solution.

TPP-LND NPs and TPP-LND-DOX NPs were prepared as the above method. 200 μL of the TPP-LND/MeOH solution was dropped into 5 mL of aqueous water and kept stirring at 1000 rpm for 5 min. After that, the MeOH was removed by centrifugation (10000 rpm, 20 min) three times. When preparing TPP-LND-DOX NPs, we added 200 μL of the TPP-LND/MeOH solution and 150 μL of the DOX/DMSO solution into water at the same time. The solution was treated in the same way.

Finally, 500 μL of 1.0 mg/mL methoxy-PEG-carboxymethy (mPEG-COOH) aqueous solution were added to 10 mL of the prepared TPP-LND-DOX NPs solution. The mixed solution was subject to ultrasonic for 5 min followed by set aside for 1 h incubation at room temperature to get PEG-NPs solution. The concentrations of LND and DOX in different formulations were measured by UV-VIS Spectrophotometer (U-3900, Hitachi, Japan).

4. 5. Characterization

The ^{1}H NMR spectra were collected in DMSO-d_6 on Varian 400 MHz spectrometer. SEM image was obtained with scanning electron microscopy (Carl Zeiss AG, Carl Zeiss, Germany). TEM image and EDX were obtained with transmission electron microscopy (FEI Tecnai G2 F20 S-TWIN, FEI, U.S.A.). The average sizes and zeta potentials of nanoparticles were measured through Zetasizer Nano ZS (Malvern Instruments, Malvern, U.K.).

4.6. *In vitro* release of DOX

2 mL of TPP-LND-DOX NPs and PEG-TPP-LND-DOX NPs solutions were injected into separate dialysis cartridges (MWCO 10 kDa), then these cartridges were immersed into 100 mL of PBS with pH 6.3 and pH 7.4, individually, and kept stirring at 37 °C. At desired time intervals, 1 mL of solution was collected from each sample for fluorescence measurement and the dialysis medium was replenished with an equal volume of fresh one. The amount of the released DOX was measured by determining its absorbance at 496 nm. The experiments were performed in 3 replicates and the average was used in quantitative analysis.

4. 7. Cell culture

HeLa cells were cultured in Dulbecco's Modified Eagle Medium (DMEM), while 4T1, MCF-7, multidrug resistant MCF-7 (MCF-7/ADR) cells were cultured in Roswell Park Memorial Institute (RPMI) 1640 medium. All of the cell culture media were with 10% FBS and 1% penicillin/streptomycin solution. Cells were incubated at 37 °C under 5% CO_2 atmosphere.

4. 8. *In Vitro* Studies

4. 8. 1. *In vitro* cellular uptake and bioimaging

All the HeLa cells with a density of 1×10^5 cells/mL were seeded on 35 mm glass-bottomed dishes at 37 °C in a 5% CO_2 atmosphere. With 48 h incubation, the cells were treated with the mixture of free TPP-LND and DOX molecules (TPP-LND+DOX), and TPP-LND-DOX NPs for 4, 8, 12, 16, and 20 h under 5% CO_2 at 37 °C after washed with PBS twice. The final concentration of LND and DOX were both 5 μg/mL. The cells were stained with Hoechst 33258 after being washed with PBS for two times. After 1 h incubation, the cells were washed with PBS two times and stained with Mito-Tracker Green (Beyotime, Shanghai agent, China) for 30

min under 5% CO_2 at 37 °C. Cell images were collected on a confocal microscope (Leica, model TCS SP5). Cell division studies appeared during the cellular uptake progress.

4. 8. 2. *In vitro* cytotoxicity

4T1 cells, MCF-7 cells, MCF-7/ADR cells, and HL7702 cells were seeded in 96-well plates of 8×10^3 cells per well. After 24 h under 5% CO_2 at 37 °C, the culture medium was replaced with fresh medium which contained varying concentrations of DOX NPs, TPP-LND NPs, mixture of free TPP-LND and DOX molecules (TPP-LND+DOX), and TPP-LND-DOX NPs followed by further incubation for 24 and 48 h. The concentrations of both LND and DOX were maintained the same in all groups if contained, ranging from 0 to 12 μg/mL. Once complete the incubation, all drug solutions were removed and the cells were washed in PBS twice. Subsequently, 20 μL of MTT (5 mg/mL) were added into each well, followed by 4 h incubation. Finally, MTT solution was cleaned up and replaced with 150 mL of DMSO per well, leaving for dissolution for 15 min, and then the absorbance at 570 nm of each well was measured on a Bio-Rad microplate reader (Bio-Rad, Hercules, CA, USA) to determine cell viability. The cytotoxicity of free DOX molecules on MCF-7 cells and MCF-7/ADR cells was measured with the same procedure as described above.

4. 8. 3. Detection of ROS

4T1, and MCF-7/ADR cells were seeded in 35 mm glass-bottomed dishes and treated with DOX NPs, TPP-LND NPs, mixture of free TPP-LND and DOX molecules (TPP-LND+DOX), and TPP-LND-DOX NPs under 5% CO_2 at 37 °C. The control experiment was blank culture medium. After 12 and 24 h incubation, the culture medium was removed and cells were washed with PBS for two times, then the cells were stained with DCFH-DA (Beyotime, Shanghai agent,

China) for 20 min under 5% CO_2 at 37 °C. Cell images were collected on a confocal microscope. The concentrations of both LND and DOX were 10 μg/mL.

4. 8. 4. Mitochondrial membrane potential (Δψm) depolarization

4T1, and MCF-7/ADR cells were seeded in 35 mm glass-bottomed dishes and treated with DOX NPs, TPP-LND NPs, mixture of free TPP-LND and DOX molecules (TPP-LND+DOX), and TPP-LND-DOX NPs under 5% CO_2 at 37 °C. The control experiment was blank culture medium. After 12 and 24 h incubation, the culture medium was removed and cells were washed with PBS for two times, then the cells were stained with Rhodamine 123 (Beyotime, Shanghai agent, China) for 30 min under 5% CO_2 at 37 °C. Cell images were collected on a confocal microscope. The concentrations of both LND and DOX were 10 μg/mL.

4. 8. 5. Western blot analysis

The protein expression of mitochondria apoptosis was measured following a previous report.[42] 4T1 cells were seeded in 6-well plates for 24 h incubation and were treated with different formulations (free LND, free TPP-LND, DOX NPs, TPP-LND NPs, mixture of free TPP-LND and DOX molecules (TPP-LND+DOX), and TPP-LND-DOX NPs). After 24 h incubation, the proteins were tested by BCA Protein Assay Kit (Sigma, Shanghai, China) and visualized by enhanced chemiluminescence (ECL) Western blotting detection reagents (Peiqing, Shanghai Peiqing Science&Technology, China). The concentrations of both LND and DOX were 10 μg/mL.

4. 9. *In vivo* studies

4. 9. 1. Blood circulation

BALB/c nude mice were split to two groups and one was injected with 200 μL of mPEG-COOH modified PEG-TPP-LND-DOX NPs through intravenous injection. The blood samples were collected from tail vein at different time intervals (0, 5, 10, and 30 min; and 1, 2, 4, 6, 8, 12, and 24 h). Each blood sample was approximately 15 μL and dissolved in 1 mL of lysis buffer. The circulation of drugs was measured by testing the fluorescence intensities of DOX at 555 nm on a F-4600 FL spectrophotometer. The blood of mice without drug injection was used as blank control group to cleaning up the autofluorescence of blood at 555 nm. A series of DOX solution with various concentrations were measured to make a standard calibration curve.

4. 9. 2. Biodistribution

MCF-7/ADR bearing BALB/c nude mice were injected with 200 μL of the mixture of free PEG-TPP-LND and DOX molecules (PEG-TPP-LND+DOX), and PEG-TPP-LND-DOX NPs via tail vein. Both concentrations of LND and DOX were maintained at 1 mg/mL. Mice were sacrificed after 24 h injection. We measured the *in vivo* fluorescence intensity of each organ by Maestro system, and then the fluorescence intensity was converted into the quantity of DOX by a standard fluorescence curve after deducting the background fluorescence of the tissues and organs of the mice without drug treatment. Laser at 496 nm was used as excitation wavelength, and spectral imaging from 530 to 630 nm was collected. Then, we weighed the tissues and organs, and finally the percentage of DOX in total dose per gram of tissue was calculated (% ID/g).

4. 9. 3. *In vivo* antitumor activity

MCF-7/ADR bearing BALB/c nude mice were divided into 5 groups when the tumors grouped up to about 80-100 mm^3, and intravenously administrated by 200 μL of PBS, PEG-DOX

NPs, PEG-TPP-LND NPs, the mixture of free PEG-TPP-LND and DOX molecules (PEG-TPP-LND+DOX), and PEG-TPP-LND-DOX NPs, both concentrations of LND and DOX were maintained at 1 mg/mL. The same therapy was implemented at day 7. We measured the tumor size and body weight of mice every day during the treatment for two weeks.

4.10. Statistical analysis

The data are given as Mean ± S.D. Statistical significance was tested by two-tailed Student's t-test or one-way ANOVA. Statistical significance was set at $*P < 0.05$ while extreme significance was set at $**P < 0.01$.

Associated Content

Supporting Information

^{1}H NMR spectra of TPP-NH_2, LND, TPP-LND, DOX, and TPP-LND-DOX NPs. EDX of TPP-LND-DOX NPs. The release profiles of DOX from TPP-LND-DOX NPs and PEG-TPP-LND-DOX NPs. Confocal microscopy images of HeLa cells treated with mixture of free TPP-LND and DOX molecules (TPP-LND+DOX), and TPP-LND-DOX NPs for 20 h. *In vitro* toxicities of 4T1, and HL7702 cells treated with DOX NPs, TPP-LND NPs, mixture of free TPP-LND and DOX molecules (TPP-LND+DOX), and TPP-LND-DOX NPs for 24 h and 48 h. Cell viabilities of MCF-7 cells and MCF-7/ADR cells treated with free DOX molecules for 24 and 48 h. ROS and $\Delta\psi m$ of MCF-7/ADR cells treated with DOX NPs, TPP-LND NPs, mixture of free TPP-LND and DOX molecules (TPP-LND+DOX), and TPP-LND-DOX NPs for 12 h and 24 h. This material is available free of charge via the Internet at http://pubs.acs.org.

Author Information

Corresponding Author

* (X. J. Z.) Tel: +86-512-65880955. E-mail: xjzhang@suda.edu.cn;

* (X. H. Z.) Tel: +86-512-65882631. E-mail: xiaohong_zhang@suda.edu.cn.

Notes

The authors declare no competing financial interest.

Acknowledgment

This research was financially supported by the National Basic Research Program of China (2013CB933500), National Natural Science Foundation of China (Grant No. 61422403, 51672180, 51622306, 21673151), Qing Lan Project, Collaborative Innovation Center of Suzhou Nano Science and Technology (NANO-CIC), and the Priority Academic Program Development of Jiangsu Higher Education Institutions (PAPD).

References

(1) Ghobrial, I. M.; Witzig, T. E.; Adjei, A. A. Targeting apoptosis pathways in cancer therapy, *CA Cancer J Clin*. **2005**, *55*, 178-194.

(2) Gupta, S.; Kass, G. E. N.; Szegezdi, E.; Joseph, B. The mitochondrial death pathway: a promising therapeutic target in diseases, *J. Cell. Mol. Med.* **2009**, *13*, 1004-1033.

(3) Matt, S.; Hofmann, T. G. The DNA damage-induced cell death response: a roadmap to kill cancer cells, *Cell. Mol. Life Sci.* **2016**, *73*, 2829-2850.

(4) Hodkinson, P. S.; Elliott, T.; Wong, W. S.; Rintoul, R. C.; Mackinnon, A. C.; Haslett, C.; Sethi, T. ECM overrides DNA damage-induced cell cycle arrest and apoptosis in small-cell lung cancer cells through b1 integrin-dependent activation of PI3-kinase, *Cell Death Differ*. **2006**, *13*, 1776-1788.

(5) Chen, Y. M.; Liu, X. M.; Pisha, E.; Constantinou, A. I.; Hua, Y. S.; Shen, L. X.; Breemen, R. B. V.; Elguindi, E. C.; Blond, S. Y.; Zhang, F. G.; Bolton, J. L. A metabolite of equine estrogens, 4-hydroxyequilenin, induces DNA damage and apoptosis in breast cancer cell lines, *Chem. Res.* **2000**, *13*, 342-350.

(6) Wongrakpanich, A.; Geary, S. M.; Joiner, M. A.; Anderson, M. E.; Salem, A. K. Mitochondria-targeting particles, *Nanomedicine* **2014**, *9*, 2531-2543.

(7) Braun, R. J. Mitochondrion-mediated cell death: dissecting yeast apoptosis for a better understanding of neurodegeneration, *Front Oncol.* **2012**, *2*, 182.

(8) Jung, H. S.; Han, J. Y.; Lee, J. H.; Lee, J.H.; Choi, J. M.; Kweon, H. S.; Han, J. H.; Kim, J. H.; Byun, K. M.; Jung, J. H.; Kang, C. H.; Kim, J. S. Enhanced NIR radiation-triggered hyperthermia by mitochondrial targeting, *J. Am. Chem. Soc*. **2015**, *137*, 3017-3023.

(9) Han, M.; Vakili, M. R.; Abyaneh, H. S.; Molavi, O.; Lai, R.; Lavasanifar, A. Mitochondrial delivery of doxorubicin via triphenylphosphine modification for overcoming drug resistance in MDA-MB-435/DOX cells, *Mol. Pharmaceutics*. **2014**, *11*, 2640-2649.

(10) Solary, E.; Bettaieb, A.; Daloz, L. D.; Corcos, L. Mitochondria as a target for inducing death of malignant hematopoietic cells, *Leukemia & Lymphoma* **2003**, *44*, 563-574.

(11) Pelicano, H.; Martin, D. S.; Xu, R. H.; Huang, P. Glycolysis inhibition for anticancer treatment, *Oncogene* **2006**, *25*, 4633-4646.

(12) Nath, K.; Guo, L. L.; Nancolas, B.; Nelson, D. S.; Shestov, A. A.; Lee, S. C.; Roman, J.; Zhou, R.; Leeper, D. B.; Halestrap, A. P.; Blair, I. A.; Glickson, J. D. Mechanism of antineoplastic activity of lonidamine, *Biochim. Biophys. Acta, Rev. Cancer*. **2016**, *1866*, 151-162.

(13) Sordet, O.; Re´be´, C.; Leroy, I.; Bruey, J. M.; Garrido, C.; Miguet, C.; Lizard, G. Plenchette, S.; Corcos, L.; Solary, E. Mitochondria-targeting drugs arsenic trioxide and lonidamine bypass the resistance of TPA-differentiated leukemic cells to apoptosis, *Blood* **2001**, *97*, 3931-3941.

(14) Li, Y. C.; Fung, K. P.; Kwok, T. T.; Lee, C. Y.; Suen, Y. K.; Kong, S. K. Mitochondrial targeting drug lonidamine triggered apoptosis in doxorubicin-resistant HepG2 cells, *Life Sci.* **2002**, *71*, 2729-2740.

(15) Assanhou, A. G.; Li, W. Y.; Zhang, L.; Xue, L. J.; Kong, L. Y.; Sun, H. B.; Mo, R.; Zhang, C. Reversal of multidrug resistance by co-delivery of paclitaxel and lonidamine using a TPGS and hyaluronic acid dual-functionalized liposome for cancer treatment, *Biomaterials* **2015**, *73*, 284-295.

(16) Zhang, B. F.; Xing, L.; Cui, P. F.; Wang, F. Z.; Xie, R. L.; Zhang, J. L.; Zhang, M.; He, Y. J.; Lyu, J. Y.; Qiao, J. B.; Chen, B. A.; Jiang, H. L. Mitochondria apoptosis pathway synergistically activated by hierarchical targeted nanoparticles co-delivering siRNA and lonidamine, *Biomaterials* **2015**, *61*, 178-189.

(17) Li, N.; Zhang, C. X.; Wang, X. X.; Zhang, L.; Ma, X.; Zhou, J.; Ju, R. J.; Li, X. Y.; Zhao, W. Y.; Lu, W.L.; Development of targeting lonidamine liposomes that circumvent drug-resistant cancer by acting on mitochondrial signaling pathways, *Biomaterials* **2013**, *34*, 3366-3380.

(18) Lee, M. H.; Han, J. H.; Lee, J. H.; Choi, H. G.; Kang, C. H.; Kim, J. S. Mitochondrial thioredoxin-responding off-on fluorescent probe, *J. Am. Chem. Soc*. **2012**, *134*, 17314-17319.

(19) Wei, W. J.; Zhang, X. J.; Chen, X. F.; Zhou, M. J.; Xu, R. R.; Zhang, X. H. Smart surface coating of drug nanoparticles with cross-linkable polyethylene glycol for bio-responsive and highly efficient drug delivery, *Nanoscale* **2016**, *8*, 8118-8125.

(20) Zhang, J. F.; Li, Y. N.; An, F. F.; Zhang, X. H.; Chen, X. F.; Lee, C. S. Preparation and size control of sub-100 nm pure nanodrugs, *Nano Lett*. **2015**, *15*, 313-318.

(21) Zhang, J. F.; Liang, Y. C.; Lin, X. D.; Zhu, X. Y.; Yan, L.; Li, S. L.; Yang, X.; Zhu, G. Y.; Rogach, A. L.; Yu, P. K. N.; Shi, P.; Tu, L. C.; Chang, C. C.; Zhang, X. H.; Chen, X. F.; Zhang, W. J.; Lee, C. S. Self-monitoring and self-delivery of photosensitizer-doped nanoparticles for highly effective combination cancer therapy *in vitro* and *in vivo*, *ACS Nano* **2015**, *9*, 9741-9756.

(22) Yu, C. T.; Zhou, M. J.; Zhang, X. J.; Wei, W. J.; Chen, X. F.; Zhang, X. H. Smart doxorubicin nanoparticles with high drug payload for enhanced chemotherapy against drug resistance and cancer diagnosis, *Nanoscale* **2015**, *7*, 5683-5690.

(23) Zhou, M. J.; Zhang, X. J.; Yang, Y. L.; Liu, Z.; Tian, B. S.; Jie, J. S.; Zhang, X. H. Carrier-free functionalized multidrug nanorods for synergistic cancer therapy, *Biomaterials* **2013**, *34*, 8960-8967.

(24) Stoyanovsky, D. A.; Jiang, J. F.; Murphy, M. P.; Epperly, M.; Zhang, X. L.; Li, S.; Greenberger, J.; Kagan, V.; Bayır, H. Design and synthesis of a mitochondria-targeted mimic of glutathione peroxidase, mitoEbselen-2, as a radiation mitigator, *ACS Med. Chem. Lett*. **2014**, *5*, 1304-1307.

(25) Ravagnan, L.; Marzo, I.; Costantini, P.; Susin, S. A.; Zamzami, N.; Petit, P. X.; Hirsch, F. Ë.; Goulbern, M.; Poupon, M. F.; Miccoli, L.; Xie, Z. H.; Reed, J. C.; Kroemer, G. Lonidamine triggers apoptosis via a direct, Bcl-2-inhibited effect on the mitochondrial permeability transition pore, *Oncogene* **1999**, *18*, 2537-2546.

(26) Wang, Z. C.; Wang, J.; Xie, R. F.; Liu, R. L.; Lu, Y. Mitochondria-derived reactive oxygen species play an important role in doxorubicin-induced platelet apoptosis, *Int. J. Mol. Sci*. **2015**, *16*, 11087-11100.

(27) Zhu, X. Y.; Yuen, M. F.; Yan, L.; Zhang, Z. Y.; Ai, F. J.; Yang, Y.; Yu, P. K. N.; Zhu, G. Y.; Zhang, W. J.; Chen, X. F. Diamond-nanoneedle-array-facilitated intracellular delivery and the potential influence on cell physiology, *Adv. Healthcare Mater*. **2016**, *5*, 1157-1168.

(28) Yang, Y. H.; Karakhanova, S.; Hartwig, W.; Haese, J. G. D.; Philippov, P. P.; Werner, J.; Bazhin, A. V. Mitochondria and mitochondrial ROS in cancer: novel targets for anticancer therapy, *J. Cell. Physiol*. **2016**, *231*, 2570-2581.

(29) Xiong, H.; Du, S.; Ni, J.; Zhou, J. P.; Yao, J. Mitochondria and nuclei dual-targeted heterogeneous hydroxyapatite nanoparticles for enhancing therapeutic efficacy of doxorubicin, *Biomaterials* **2016**, *94*, 70-83.

(30) Indo, H. P.; Davidson, M.; Yen, H. C.; Suenaga, S.; Tomita, K.; Nishii, T.; Higuchi, M.; Koga, Y.; Ozawa, T.; Majima, H. J. Evidence of ROS generation by mitochondria in cells with impaired electron transport chain and mitochondrial DNA damage, *Mitochondrion* **2007**, *7*, 106-118.

(31) Kuznetsov, A. V.; Margreiter, R.; Amberger, A.; Saks, V.; Grimm, M. Changes in mitochondrial redox state, membrane potential and calcium precede mitochondrial dysfunction in doxorubicin-induced cell death, *Biochim. Biophys. Acta, Mol. Cell Res*. **2011**, *1813*, 1144-1152.

(32) Theodossiou, T. A.; Sideratou, Z.; Katsarou, M. E.; Tsiourvas, D. Mitochondrial delivery of doxorubicin by triphenylphosphonium-functionalized hyperbranched nanocarriers results in rapid and severe cytotoxicity, *Pharm. Res*. **2013**, *30*, 2832-2842.

(33) Bufalo, D. D.; Biroccio, A.; Soddu, S.; Laudonio, N.; Angelo, C. D.; Sacchi, A.; Zupi, G. Lonidamine induces apoptosis in drug-resistant cells independently of the p53 gene, *J. Clin. Invest.* **1996**, *98*, 1165-1173.

(34) Zhang, B. F.; Xing, L.; Jiang, H. L. Co-delivery of siRNA and a chemotherapeutic prodrug to trigger mitochondria-mediated cancer-cell apoptosis, *Nanomedicine: NBM.* **2016**, *12*, 449-575.

(35) Sun, K.; Liu, Z. S.; Sun, Q. Role of mitochondria in cell apoptosis during hepatic ischemia-reperfusion injury and protective effect of ischemic postconditioning, *World J. Gastroenterol.* **2004**, *10*, 1934-1938.

(36) Djafarzadeh, S.; Vuda, M.; Takala, J.; Jakob, S. M. Effect of remifentanil on mitochondrial oxygen consumption of cultured human hepatocytes, *PLoS One* **2012**, *7*, 45195.

(37) Twiddy, D.; Cain, K. Caspase-9 cleavage, do you need it?, *Biochem. J.* **2007**, *405*, e1-e2.

(38) Maeda, H.; Wu, J.; Sawa, T.; Matsumura, Y.; Hori, K. Tumor vascular permeability and the EPR effect in macromolecular therapeutics: a review, *J. Controlled Release* **2000**, *65*, 271-284.

(39) Farokhzad, O. C.; Cheng, J. J.; Teply, B. A.; Sherifi, I.; Jon, S.; Kantoff, P. W.; Richie, J. P.; Langer, R. Targeted nanoparticle-aptamer bioconjugates for cancer chemotherapy *in vivo*, *PNAS* **2006**, *103*, 6315-6320.

(40) Zitvogel, L.; Apetoh, L.; Ghiringhelli, F.; Kroemer, G. Immunological aspects of cancer chemotherapy, *Nat. Rev.* **2008**, *8*, 59-73.

(41) Xu, R. R.; Huang, L. M.; Wei, W. J.; Chen, X. F.; Zhang, X. H.; Zhang, X. J. Real-time imaging and tracking of ultrastable organic dye nanoparticles in living cells, *Biomaterials* **2016**, *93*, 38-47.

(42) Martinou, J. C.; Desagher, S.; Antonsson, B. Cytochrome c release from mitochondria: all or nothing, *Nat. Cell. Biol.* **2000**, *2*, E41-E43.

Table of Contents Image

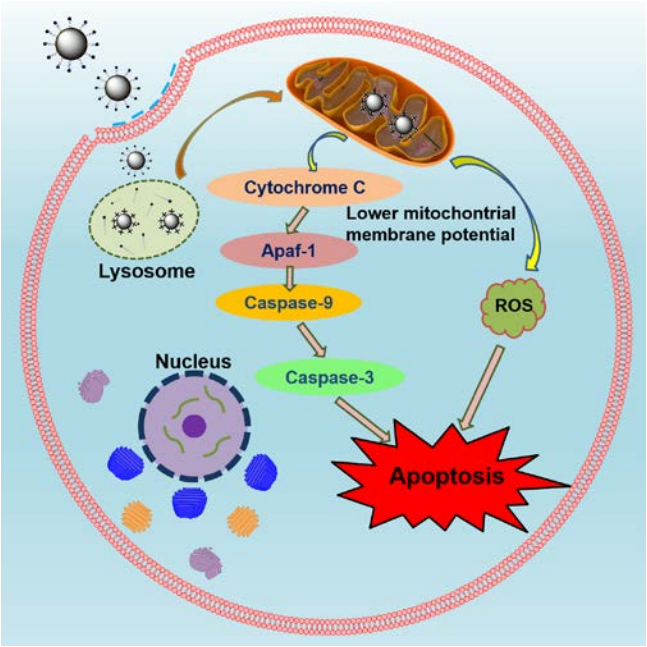

Supporting Information

Mitochondrial Targeting Lonidamine-Doxorubicin Nanoparticles for Synergistic Chemotherapy to Conquer Drug Resistance

Yanqiu Liu,[+] *Xiujuan Zhang,*[*,+] *Mengjiao Zhou,*[+] *Xueyan Nan,*[+] *Xianfeng Chen,*[‡] *Xiaohong Zhang*[*,+]

[+]Institute of Functional Nano & Soft Materials (FUNSOM) and Jiangsu Key Laboratory for Carbon-Based Functional Materials & Devices, Soochow University, Suzhou Jiangsu, 215123 (P. R. China)

[‡]School of Engineering, Institute for Bioengineering, University of Edinburgh, Edinburgh EH9 3JL, United Kingdom.

Corresponding Author

* (X. J. Z.) Tel: +86-512-65880955. E-mail: xjzhang@suda.edu.cn;

* (X. H. Z.) Tel: +86-512-65882631. E-mail: xiaohong_zhang@suda.edu.cn.

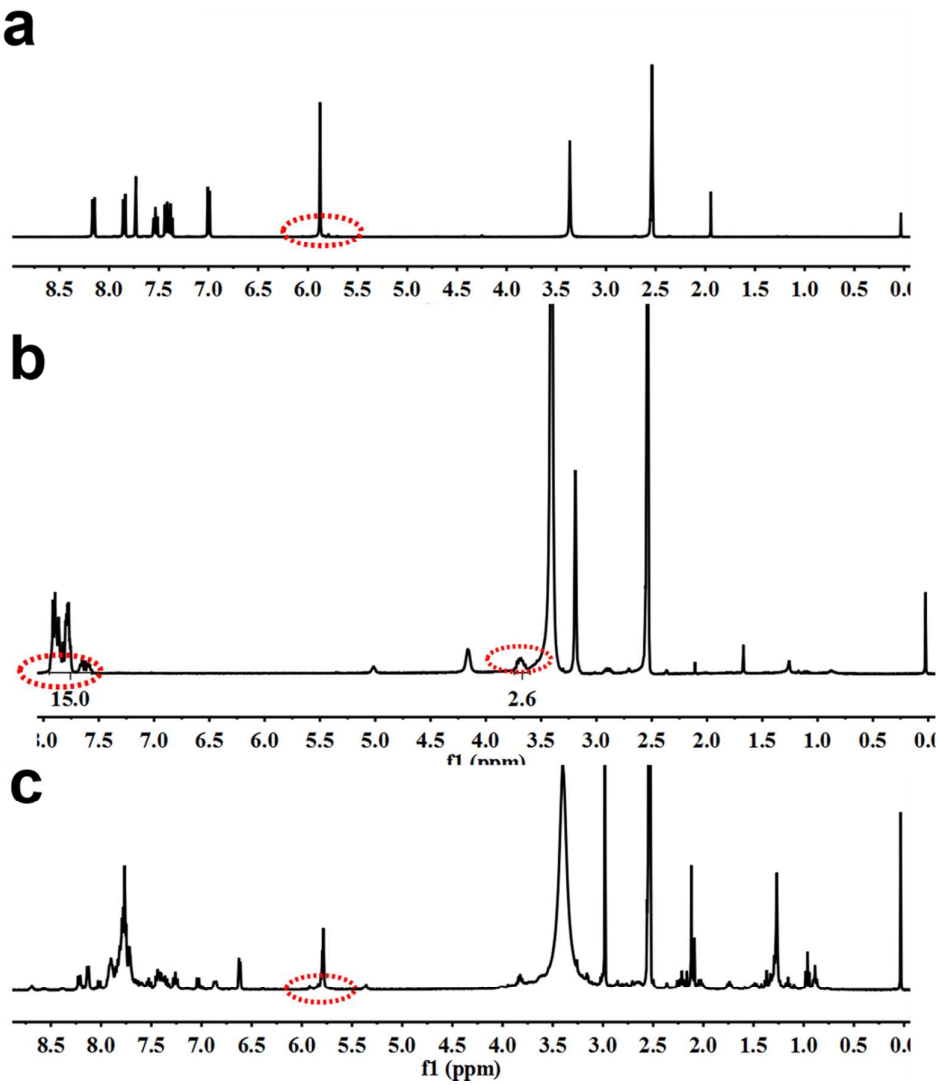

Figure S1. ^{1}H NMR spectrum of (a) LND, (b) TPP-NH_2, (c) TPP-LND.

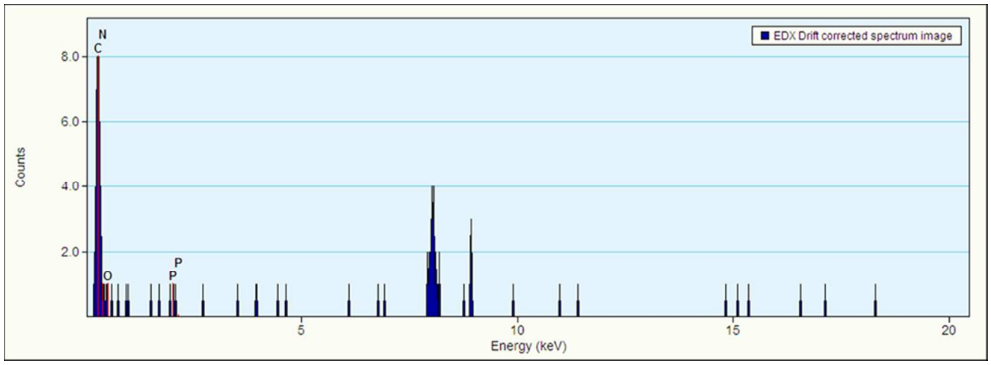

Figure S2. The energy-dispersive X-ray spectroscopy (EDX) of naked TPP-LND-DOX NPs.

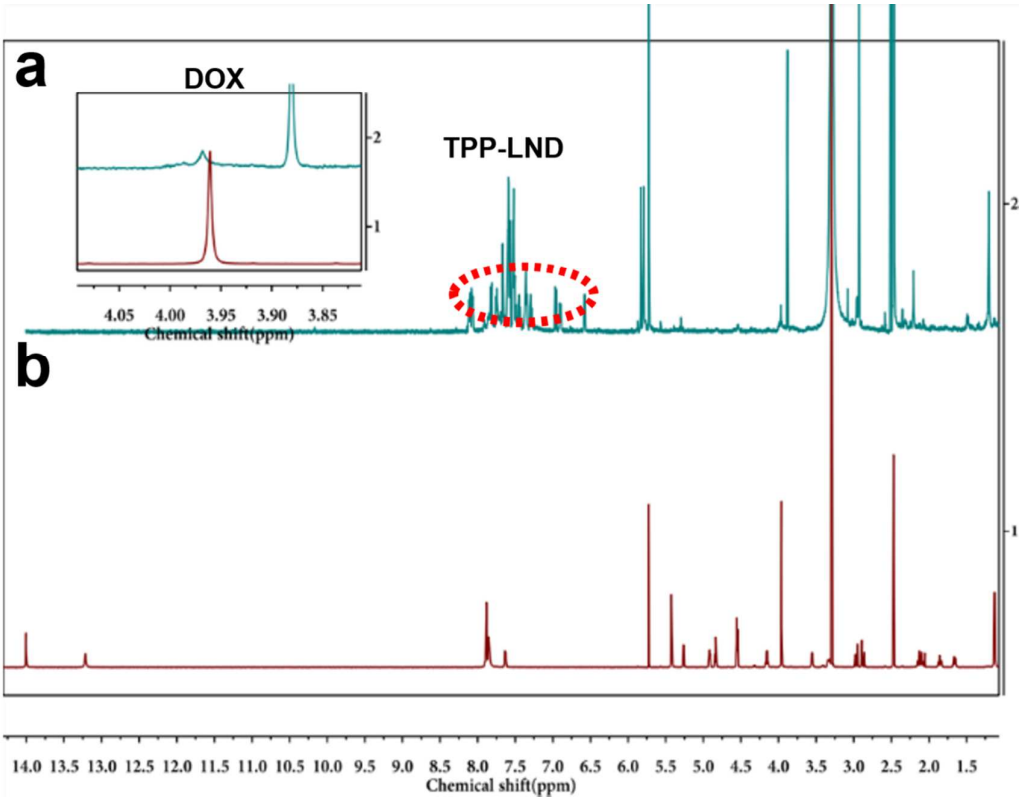

Figure S3. ^{1}H NMR spectrum of (a) TPP-LND-DOX NPs, and (b) DOX molecules. The peak of 3.96 is the -OCH_3 of DOX, and the peak from 7.0 to 8.0 corresponds to the benzene of TPP-LND.

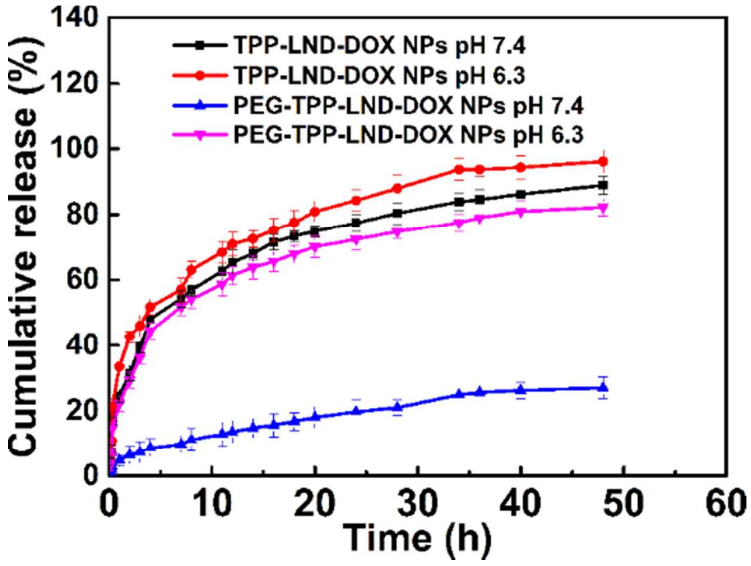

Figure S4. The release profiles of DOX from TPP-LND-DOX NPs and PEG-TPP-LND-DOX NPs at pH 7.4 and 6.3.

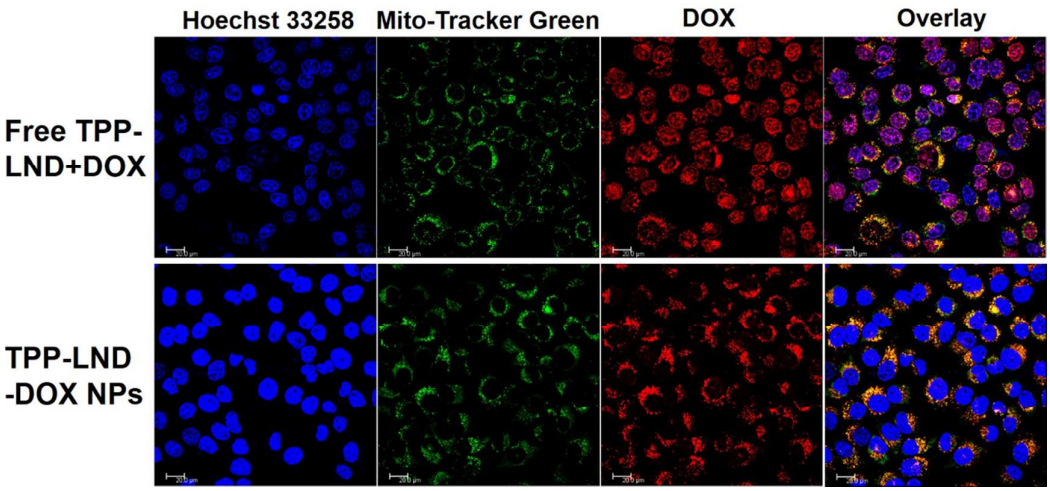

Figure S5. Cellular uptake and intracellular distribution of the mixture of free TPP-LND and DOX molecules (TPP-LND+DOX) and TPP-LND-DOX NPs in HeLa cells. The confocal fluorescence microscopy images of intracellular localization of the NPs in HeLa cells were observed at 24 h incubation with free TPP-LND+DOX and TPP-LND-DOX NPs. Scale bar: 20 μm. Hoechst 33258 and Mito-Tracker Green were used to stain the nuclei and mitochondria of cells, respectively.

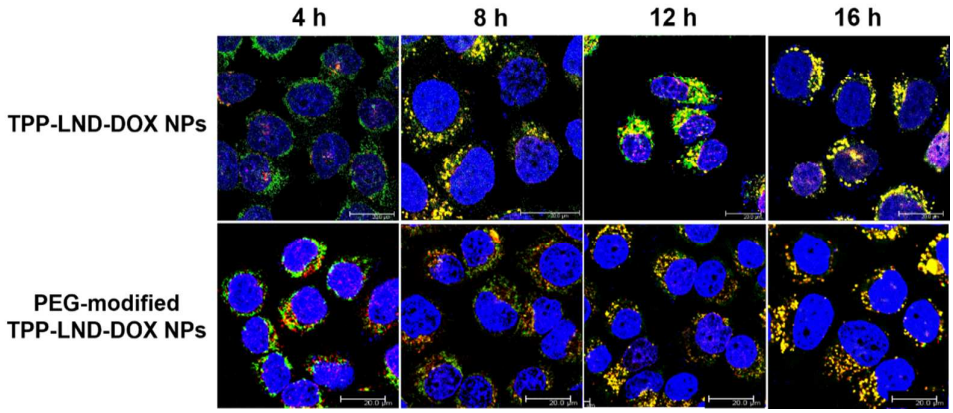

Figure S6. Fluorescence images of HeLa cells after being incubated with TPP-LND-DOX NPs with/without PEG surface modification for different times. The scale bars indicate 20 μm. Hoechst 33258 and Mito-Tracker Green were used to stain the nuclei and mitochondria of cells, respectively. NPs, mitochondria and nucleus are shown in red, green, and blue, respectively.

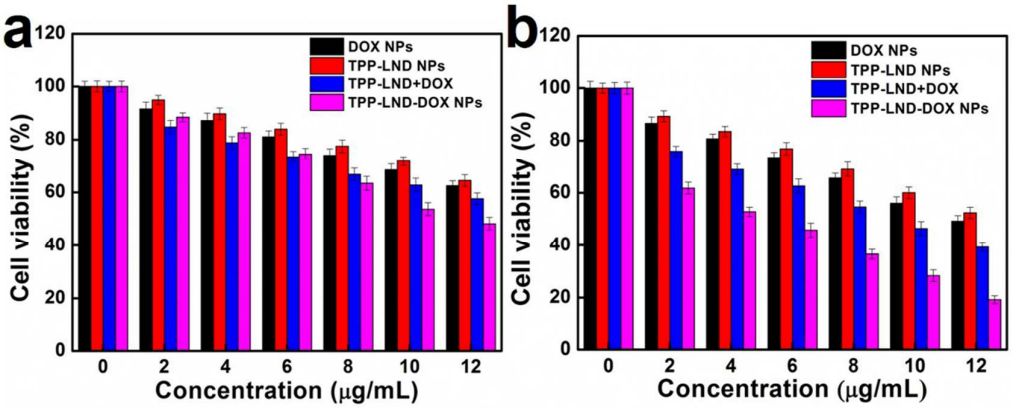

Figure S7. Cell viabilities of 4T1 cell lines after being incubated with DOX NPs, TPP-LND NPs, mixture of free TPP-LND and DOX molecules (TPP-LND+DOX), and TPP-LND-DOX NPs for 24 (a) and 48 (b) h.

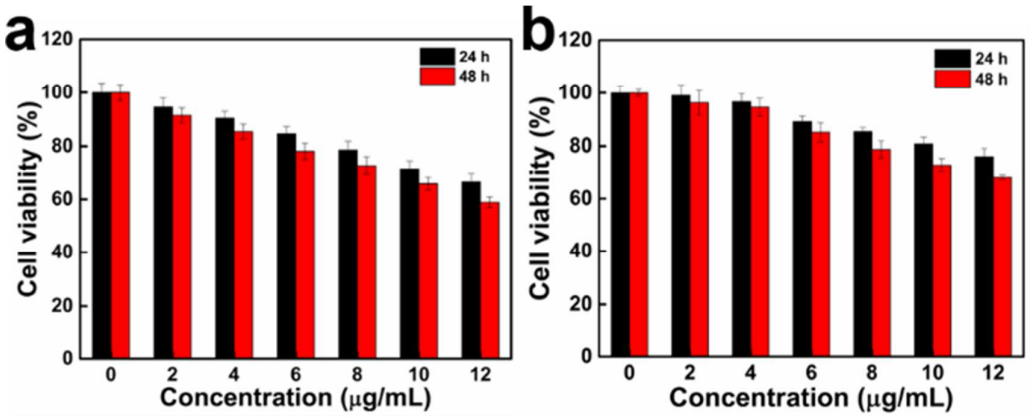

Figure S8. Cell viabilities of MCF-7 cell lines (a) and MCF-7/ADR cell lines (b) after being incubated with free DOX molecules, for 24 and 48 h.

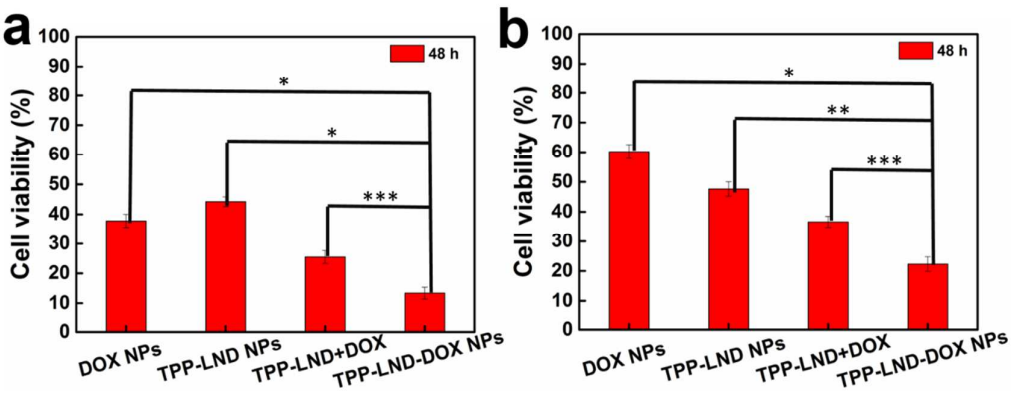

Figure S9. Cell viabilities of MCF-7 (a) and MCF-7/ADR (b) cells after being incubated with 12 μg/mL of DOX NPs, TPP-LND NPs, mixture of free TPP-LND and DOX molecules (TPP-LND+DOX), and TPP-LND-DOX NPs for 48 h. Asterisks (*) denote statistically significant differences calculated by one-way ANOVA test, *$p < 0.001$, **$p < 0.02$, ***$p < 0.05$.

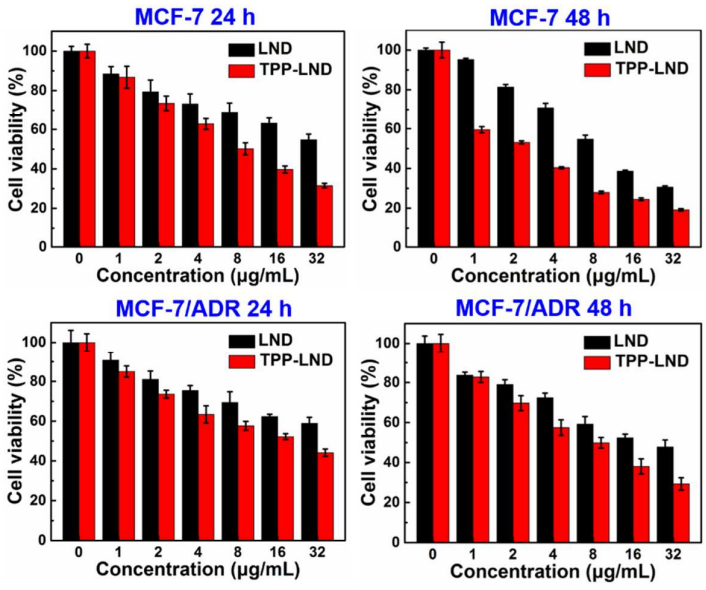

Figure S10. The cytotoxicity of free LDN and covalently conjugated TPP-LND to MCF-7 cancer cells and MCF-7/ADR cancer cells. The concentrations of LND were maintained the same in both groups, ranging from 0 to 32 μg/mL.

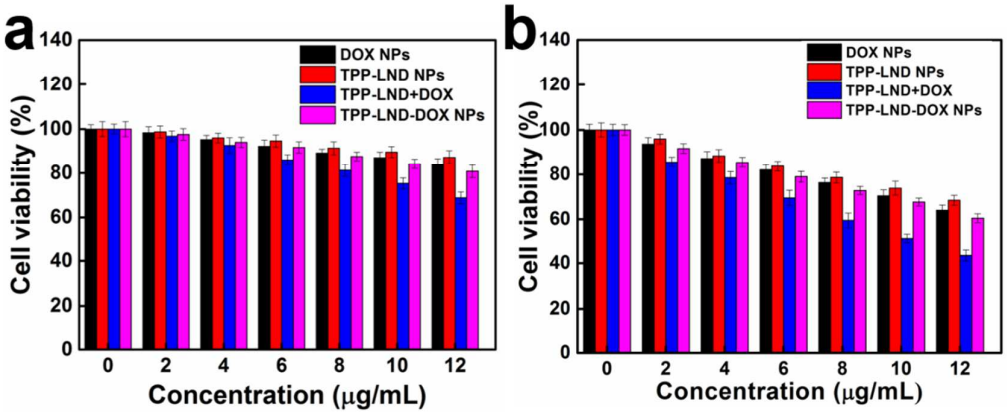

Figure S11. Cell viabilities of normal human liver cells (HL7702 cells) after being incubated with different concentrations of DOX NPs, TPP-LND NPs, mixture of free TPP-LND and DOX molecules (TPP-LND+DOX), and TPP-LND-DOX NPs for 24 and 48 h. The concentrations of both LND and DOX in were maintained the same, ranging from 0 to 12 μg/mL.

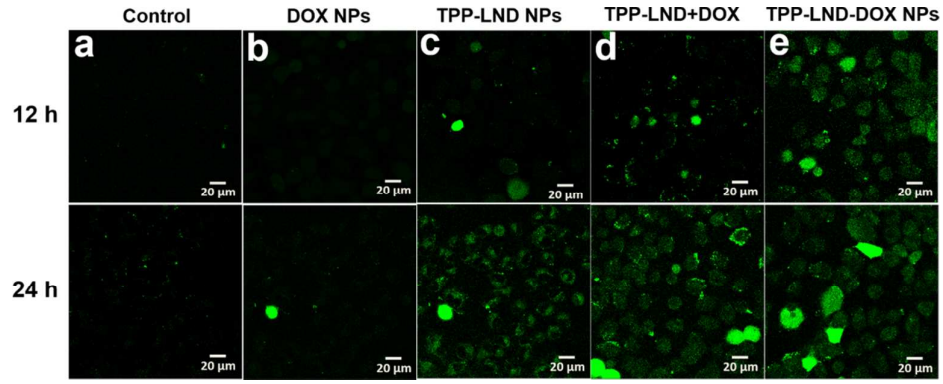

Figure S12. Reactive oxygen species (ROS) generation in MCF-7/ADR cells treated with different drugs. The confocal fluorescence microscopy images of (a) untreated cells, and the cells incubated with (b) DOX NPs, (c) TPP-LND NPs, (d) free TPP-LND and DOX molecules (TPP-LND+DOX), and (e) TPP-LND-DOX NPs for 12 and 24 h. Scale bar: 20 μm. The concentrations of both LND and DOX were maintained at 10 μg/mL.

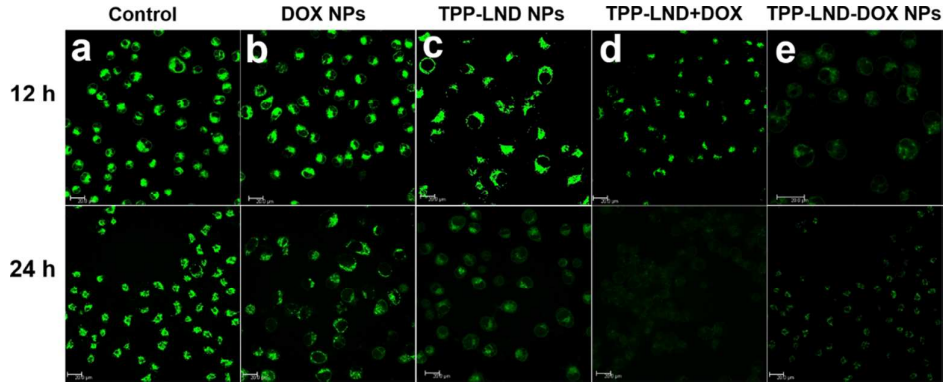

Figure S13. The mitochondrial membrane potential (Δψm) depolarization of MCF-7/ADR cells cultured with (b) DOX NPs, (c) TPP-LND NPs, (d) free TPP-LND and DOX molecules (TPP-LND+DOX), and (e) TPP-LND-DOX NPs for 12 and 24 h, (a) The control experiment. Scale bar: 20 μm. The concentrations of both LND and DOX were maintained at 10 μg/mL.